Nonlinear rocket motor stability prediction: Limit amplitude, triggering, and mean pressure shift[a)]

Gary A. Flandro, Sean R. Fischbach, and Joseph Majdalani[b)]
Department of Mechanical, Aerospace and Biomedical Engineering, University of Tennessee (UTSI), Tullahoma, Tennessee 37388-9700, USA

(Received 23 January 2007; accepted 24 April 2007; published online 5 September 2007)

High-amplitude pressure oscillations in solid propellant rocket motor combustion chambers display nonlinear effects including: (1) *limit cycle behavior* in which the fluctuations may dwell for a considerable period of time near their peak amplitude, (2) elevated mean chamber pressure (*DC shift*), and (3) a *triggering* amplitude above which pulsing will cause an apparently stable system to transition to violent oscillations. Along with the obvious undesirable vibrations, these features constitute the most damaging impact of combustion instability on system reliability and structural integrity. The physical mechanisms behind these phenomena and their relationship to motor geometry and physical parameters must, therefore, be fully understood if instability is to be avoided in the design process, or if effective corrective measures must be devised during system development. Predictive algorithms now in use have limited ability to characterize the actual time evolution of the oscillations, and they do not supply the motor designer with information regarding peak amplitudes or the associated critical triggering amplitudes. A pivotal missing element is the ability to predict the mean pressure shift; clearly, the designer requires information regarding the maximum chamber pressure that might be experienced during motor operation. In this paper, a comprehensive nonlinear combustion instability model is described that supplies vital information. The central role played by steep-fronted waves is emphasized. The resulting algorithm provides both detailed physical models of nonlinear instability phenomena and the critically needed predictive capability. In particular, the origin of the DC shift is revealed.
[DOI: 10.1063/1.2746042]

I. INTRODUCTION

Combustion instability in solid propellant rocket motors is frequently associated with sonic waves, since measured frequencies are closely approximated by simple acoustic theory. For this reason, analytical work aimed at providing physical insight into the phenomenon is, quite naturally, founded upon the notion of perturbed acoustic waves.[1–8] All predictive codes are built upon these concepts.[2–4,6–16] This includes the SSP (Standard Stability Prediction program) now used almost universally in treating instability problems. Most such predictive algorithms represent only the *linear* features of the instability, and provide no information regarding important nonlinear features of great practical significance.

A typical SSP calculation yields only a set of growth rates based on the underlying linear theory. Usually these are net growth rates for each acoustic mode and burn time selected by the analyst. If, for example, all of these are found to be negative, then the system is deemed to be stable. If one (or more) is positive, the user interprets this to mean that there is a potential instability problem. That is, there may be a *tendency* for the motor to oscillate. No information is forthcoming regarding what amplitude such oscillations are likely to attain, or whether or not the system is susceptible to triggered instability initiated by random or deliberate pulsing.

The *limit cycle*, or peak amplitude reached by the oscillations, is obviously an important quantity since it reflects the vibration environment produced by the instability. Attempts have been made to understand this limiting behavior of the wave system by including nonlinear corrections that extend the linear acoustic instability theories.[5,6,17–22] These efforts have been useful in demonstrating certain essential physical phenomena, such as the natural steepening mechanism that causes initially low-amplitude acoustic waves to transition into shock-like structures.[5,17,19,20,23–25] The central role played by shock waves in nonlinear longitudinal mode combustion instability has also been convincingly demonstrated experimentally.[26]

More importantly, no information is provided regarding the much dreaded *DC shift*, or mean pressure excursion that often accompanies finite amplitude oscillations. It is curious that although the DC shift was, historically, the first observed sign of combustion instability, its true origin and its exact nature have never been successfully established.[12,27,28] Therefore, considerable attention is devoted in this paper to rectifying this situation. In particular, we seek to understand in detail its obvious connection to the oscillatory gas motions and the controlling factors in terms of chamber geometry and physical parameters.

[a)]This paper was first presented as AIAA Paper 2004-4054 at the 40th AIAA/ASME/SAE/ASEE Joint Propulsion Conference and Exhibit, Fort Lauderdale, Florida, 11–14 July 2004 and was the winner of the 2004 AIAA Solid Rockets Best Paper award.

[b)]Author to whom all correspondence should be addressed. Electronic mail: drmajdalani@gmail.com

In this paper we apply a new set of analytical tools that have evolved from many decades of struggle with the solid propellant rocket combustion instability problem. Recent work by the present authors has led to considerable progress in the development and refinement of predictive capability. To be useful, such tools must go far beyond the usual linear growth rate calculations. To be complete, the analysis must account for:

- Steep-fronted, shocked pressure waves.
- Effects of rotational flow interactions.
- Combustion coupling including distributed energy release and surface interactions.
- Mean pressure shift and its coupling with the oscillatory flowfield.

Each of these elements receives due consideration in the approach detailed in this and supporting papers.[29–31] Therein, application of the new analysis in prediction, diagnosis and correction of solid rocket motor behavior is described in detail. Its validity will be tested by comparing results to experimental data from several previous studies[12,27,28,32,33] to be described in the next section.

II. EXPERIMENTAL OBSERVATIONS

This section highlights nonlinear combustion instability attributes as they appear in experimental data. The shortcomings of the linearized analytical tools will become quite apparent. Research teams have almost universally understood the importance of the nonlinear features so clearly portrayed in test data. This has motivated some excellent work in extending the analytical basis and also in devising improved experimental techniques to take advantage of the richer set of data when nonlinearity is present. What is presented here is of necessity limited to a few key cases; there have, of course, been major contributions by many other investigators.

Figure 1 depicts typical nonlinear combustion instability effects in a combustor undergoing high-amplitude pressure fluctuations. Data from a pressure gauge with low-frequency resolution is depicted in Fig. 1(a); both the DC pressure rise and the limit cycle are clearly in evidence. Figure 1(b) shows the corresponding waveform measured by high-frequency instrumentation. The steep-fronted nature of the wave is evident. Although this is a shock-like unsteady flow, the measured frequency is closely matched by the first longitudinal acoustic mode. The spectrum is illustrated in Fig. 1(c). The first peak is the 1L (first longitudinal) acoustic frequency, and subsequent peaks correspond to the harmonics. The practiced solid motor combustion instability analyst could easily be convinced that the data shown are from an unstable tactical motor firing. However, it happens that these data are from an unstable *liquid engine preburner*.[30] It is used here to point out the important fact that all of the nonlinear features we seek to understand can be found in many types of combustors and industrial burners. Companion papers[30,31] describe the nonlinear behavior observed in liquid rocket engines. The reader should note that there is much potential benefit in a parallel treatment of these difficult problems since there is so much commonality. Unfortunately, there has been little transfer of knowledge between the liquid, solid, and jet engine research communities that deal with combustion instability development problems.

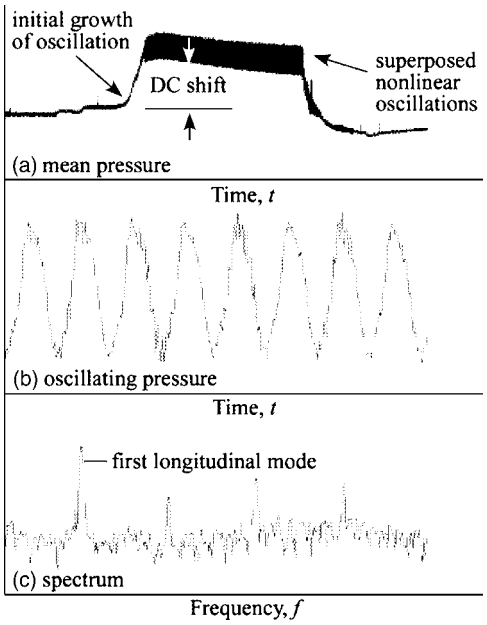

FIG. 1. Nonlinear instability effects.

A. Nonlinear T-burner experiments

We begin with a short description of some excellent work conducted by Jensen and Beckstead[34] in their attempt to better characterize nonlinear features seen in T-burner test results. Curiously, this very promising technique was never adopted by the solid rocket industry; even more distressing, with one notable exception,[19] the combustion instability research community seems to have overlooked it completely.

The reader is reminded that a crucial parameter in the analysis of solid motor instability is the burning surface response function or admittance function. Due to the complexity of the unsteady combustion processes in solid propellants, it is still necessary to determine the response function experimentally. Thus, any predictive effort is only as good as the burner data and data reduction used to characterize the pro-

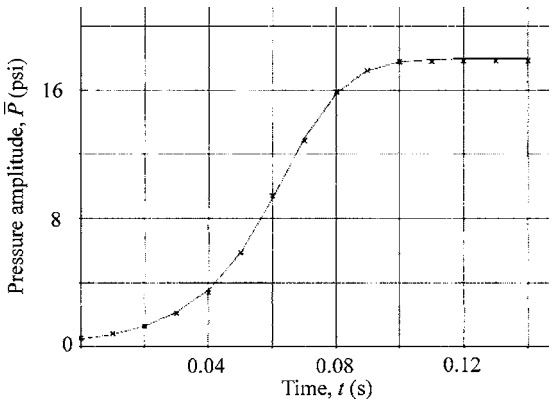

FIG. 2. Transition to limit cycle in T-burner [Jensen and Beckstead (Ref. 34)].

pellant. The T-burner has been the most successful device used for securing this vital information. However, the data is usually reduced using only the linear stability model although, as we shall demonstrate, there is much evidence that nonlinear effects are present that render the linear interpretation suspect.

Jensen and Beckstead[34] focused on the limit cycle behavior seen in burner data, and attempted to take it into account when extracting response function data. Little was known at the time of mechanisms leading to amplitude limiting, so it was assumed that nonlinear particle damping might account for the observations. Figure 2 shows typical pressure data taken in the experimental program. The most successful approach to representing this data was to assume that the rate of change of the fluctuating pressure amplitude dR/dt, is a simple nonlinear function of the amplitude, R. Jensen and Beckstead wrote:

$$\frac{1}{R}\frac{dR}{dt} = \alpha + \beta R, \tag{1}$$

where α is the linear growth rate, and β represents the effects of nonlinear damping. The solid line in Fig. 2 is a plot of an optimized curve fit of Eq. (1) to the data points shown. The fit is excellent, apparently indicating that although Eq. (1) was based on an *ad hoc* "nonlinear oscillator" analytical approach, it clearly reflects the actual nonlinear mechanisms governing the system behavior. Note that a distinct limit amplitude appears, and this is related to the coefficients by means of the simple correlation

$$\Pi = \frac{\alpha/f}{R_\infty/\bar{P}} = \beta\frac{\bar{P}}{f}, \tag{2}$$

which is found from Eq. (1) by assuming that limiting takes place when the amplitude no longer changes with time. The frequency f and mean pressure $\bar{P}$ are used to nondimensionalize the several groups of terms. It was found that the quantity Π (symbol π used in Jensen and Beckstead[34]) was very nearly a constant for many sets of data. Its numerical value was in the neighborhood of 0.5. Please note that in this model, both the linear growth rate α and nonlinear coefficient β are regarded as *unknown* parameters to be found from the experimental data as described. Assuming that the linear growth rate is correctly represented in this way, its value could then be used to deduce the propellant response function.

In a later study, Flandro[19] demonstrated that the Π correlation agreed very well with an explicit nonlinear damping mechanism representing a shock-limited nonlinear wave. The energy loss due to a steep wave front was found to be the major nonlinear damping effect rather than particle damping or nonlinear combustion. It was discovered that this shock mechanism agreed quite well with the measurements; the equivalent of the parameter β was calculated explicitly by using only the gas properties and the chamber speed of sound. This convergence of analysis and experiment guides much of what will be described in later sections of this paper.

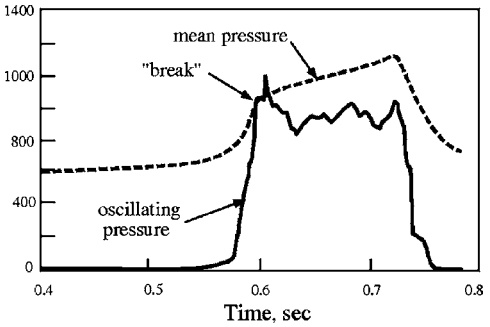

FIG. 3. Mean and oscillating pressure [Brownlee (Ref. 15)].

The following subsections describe additional observations that demonstrate in several other ways the central importance of shock waves in nonlinear instability.

B. Resonating gas columns with shock waves

In a classical experiment, Saenger and Hudson[35] demonstrated in a simple laboratory device every feature of solid rocket motor instability. A piston oscillating at the first mode acoustic frequency drove a periodic shock wave traveling back and forth in a tube. The tube length was 11 ft. and the piston displacement was only 1/8 in. Pressure measurements established that although the frequency agreed with acoustic standing wave theory, the wave was steep-fronted. For the present discussion, the most important feature of this experiment was the observation of a net change in the pressure in the closed pipe. This is in every respect analogous to the DC shift accompanying resonant oscillations in unstable rockets. In other words, the mechanism driving the steep waves simultaneously leads to a mean pressure shift. This is very useful information and, as we will demonstrate, fully supports the physical mechanism to be set forth in a later section that illuminates the origin of the DC shift in nonlinear rocket instability.

C. Brownlee's nonlinear instability experiments

In several research programs, beginning with his Ph.D. research work at Caltech (guided by Dr. F. E. Marble and carried out at the Jet Propulsion Laboratory), Brownlee confronted most of the problems we focus on here. Motors fired in these tests closely resembled what are now described as "tactical" rocket motors.[14,15,36] The motors were clearly unstable without pulsing. Oscillations became evident only after what Brownlee described as a *delay time*. Figure 3 shows typical data with a delay time of about 0.5 s. It also shows Brownlee's mysterious *break* corresponding to the apparent cessation of growth. We will show later that the time delay is the time required for the initial growth of the oscillations from naturally occurring noise. The "break" simply represents the point at which the oscillations reach their limit cycle amplitude.

Of great significance was the observation that a DC pressure rise always accompanied the oscillations when these grew to measurable amplitude. Figure 3 shows typical data. Notice that both the mean and oscillating pressure grow and

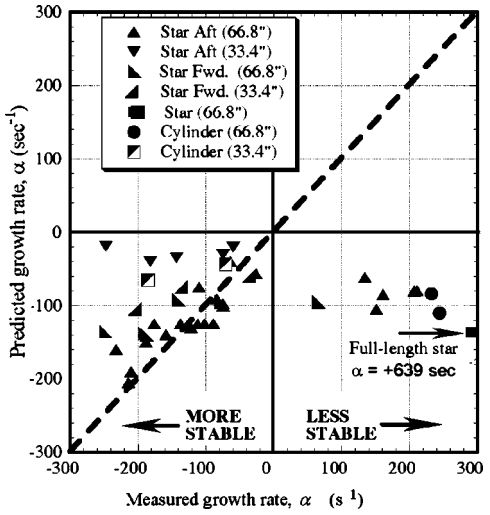

FIG. 4. Measured vs theoretical growth rates [Blomshield (Ref. 37)].

decay in exact correspondence. This is an important clue suggesting the intimate connection between these two nonlinear combustion instability phenomena.

All observations of type described must be captured analytically if useful predictive tools are to emerge. A task to be accomplished will be interpretation of Brownlee's excellent set of data using the new analytical methods to be discussed here. It would be worthwhile to devote a similar effort to other combustion instability data archives.

D. Brownlee's shockwave observations

In several carefully executed experiments, Brownlee demonstrated the importance of steep-fronted waves in solid rocket instability. Pressure histories measured in pulsed longitudinal instability clearly indicate that traveling shock-like waves characterize the nonlinear gas motions.[14] Following up with a later study, he succeeded in capturing photographically the traveling shock fronts using a windowed motor and the *schlieren* optical technique. A unique feature of the experiments was that both the propellant burning surface and the shock front could be photographed simultaneously. Brownlee[26] felt that, "…the interaction of the shock front with processes local to the burning surface should produce profound effects." Recent work in liquid rocket instability also suggests effects akin to detonation-type interactions between the steep wave system and the combustion processes.[30,31]

E. Blomshield's tactical motor tests

An extensive data set employing full-scale pulsed tactical rockets was secured in a series of heavily instrumented firings.[37] These exhibited the classical attributes of nonlinear combustion instability. Data reduction was accomplished by means of the SSP algorithm. Figure 4 shows the resulting correlation of the measured growth rates to SSP predictions. Data points on the left represent decaying pulses; those on the right are growing pulses. Note that exact agreement between the theory and experimental data is indicated when the data point lies on the diagonal line.

It is alarming that instability was never predicted by SSP; all points are placed in Fig. 4 on the negative side in terms of predicted growth rate. When data from firings that exhibited decaying pulses were compared to the SSP predictions, it was felt that acceptable agreement had been demonstrated. The authors wrote, "…in all cases the trends in measured instability were confirmed by the Standard Stability Program." However, the growing pulses indicated extremely poor agreement. The reason for this discrepancy seems clear: decaying pulses correspond to tests where negative net growth rates prevail. Therefore, as oscillations decay, they tend to approach amplitudes sufficiently small to behave in a nearly linear fashion. On the other hand, growing pulses rapidly reach amplitudes dominated by nonlinearity. It must be pointed out that, even for decaying pulses, there is strong evidence that nonlinear effects control the gas motions. Predictive capability of SSP indicated on the left side of Fig. 4 is not acceptable. Nonlinear data reduction of the sort described in the work by Jensen and Beckstead[34] is called for here.

Of even greater concern is that the linear theory does not predict the positive growth rates when pulsing leads to growing disturbances; these are correctly characterized as *triggered* instabilities. However, there is a subtle implication that there must be some basic difference between motors with growing pulses and those that decay. We will show later that this is simply related to conditions leading to positive linear growth rates. That is, these motors are made susceptible to pulsing because (despite the predictions of stability from SSP) they must be linearly unstable systems. The important message here is that there is something amiss with SSP.

The Blomshield data display all of the attributes of nonlinear behavior that were discussed in Sec. I. The spectra corresponding to growing oscillations are rich in harmonics, indicating a steepened wave structure. The DC pressure shift is closely correlated with the growth in the oscillations, and a distinct limit cycle is observed. Clearly, if such nonlinear instability is to be understood, a prerequisite must be a valid linear approximation on which to build. This theme guides the work described herein.

For emphasis, *all* motor configurations in this test series were predicted to be stable, as indicated by all points in Fig. 4 lying in the lower half of the graph. Therefore, it is the opinion of the authors that linear theory fails in accounting for Blomshield's measurements. We are challenged to find the nonlinear elements needed to explain these discrepancies in an understandable yet physically and mathematically sound manner. What is required is the ability to fully predict every feature displayed in this excellent set of data. In later sections we will demonstrate considerable progress in this undertaking.

III. ANALYSIS

Classical analyses are based on the assumption of a system of irrotational acoustic waves. Experimental data often motivates this approach, since observed oscillation frequencies are readily correlated with the standing acoustic modes of the chamber. However, assuming an acoustic basis for an instability theory results in the inability to accommodate cor-

rect boundary conditions (such as the no-slip condition at chamber boundaries) and the loss of important flow features such as unsteady vorticity that can have major impact on the validity of the results. It is also difficult to properly treat finite amplitude waves using an acoustic model. There is much evidence that the high-amplitude wave systems in unstable rockets are more akin to traveling shock fronts.[38–40] Early efforts were made to account for steepened wave effects,[5,10] but the analytical methods applied did not lead to practical solutions. These were usually based on the method of characteristics; they did not lend themselves well to generalized computational techniques of the kind needed for a practical stability assessment algorithm.

A. Failure of the SSP

The well-known failure of predictive algorithms in solid rocket analysis is largely the result of neglect of key features of the unsteady flow of combustion products. In particular, one must account for effects of vorticity production and propagation, and for the tendency of initially weak (essentially acoustic) waves to steepen into shock-like wave motions.

Solid propellant rocket motor analysis as applied in the SSP computer program, implements Culick's irrotational acoustics-based analyses.[3,4,6,11,21,41–46] As already demonstrated, this formulation does not yield satisfactory predictive capability. This is partly the result of the assumption that the wave motions are strictly acoustic (irrotational) in nature. Recent work by the writers of the present paper has focused on improving SSP by inclusion of important mechanisms such as vorticity generation and shock wave interactions. These improvements are now described briefly.

B. Rotational flow effects

Considerable progress has been made in the last decade in understanding both the precise source of the vorticity and the resulting changes in the oscillatory flow. Analytical,[42,47–55] numerical,[56–61] and experimental investigations[62–64] have demonstrated that rotational flow effects play an important role in the unsteady gas motions in solid rocket motors. Much effort has been directed to constructing the required corrections to the acoustic model. This has culminated in a comprehensive picture of the unsteady motions that agrees with experimental measurements,[42,47,48] as well as numerical simulations.[49]

These models were used in carrying out three-dimensional system stability calculations,[42,47] in a first attempt to account for rotational flow effects by correcting the acoustic instability algorithm. In this process, one discovers the origin and the three-dimensional form of the classical *flow-turning* correction; related terms appear that are not accounted for in the SSP algorithm. In particular, a rotational correction term was identified that cancels the flow-turning energy loss in a full-length cylindrical grain. However, all of these results must now be questioned because they are founded on an incomplete representation of the system energy balance.

Culick's stability estimation procedure is based on calculating the exponential growth (or decay) of an irrotational acoustic wave; the results are equivalent to energy balance models used earlier by Cantrell and Hart.[65] In all of these calculations the system energy is represented by the classical Kirchoff (irrotational and isentropic) acoustic energy density. Consequently, it does not represent the *full* unsteady field, which must include both acoustic and rotational flow effects. Kinetic energy carried by the vorticity waves is thus ignored. The actual average unsteady energy contained in the system at a given time is about 25% larger than the acoustic energy alone.[43] Furthermore, representation of the energy sources and sinks that determine the stability characteristics of the motor chamber must also be modified. Attempts to correct the acoustic growth rate model by retention of rotational flow source terms only,[42,47,55] preclude a full representation of the effects of vorticity generation and coupling.

C. Nonlinear effects

The effects of nonlinear interactions play a major role in controlling the nonlinear attributes of pressure oscillations in motor combustion chambers. Thus, strictly linearized models are of little value in the present situation. Of crucial importance is the modeling of the *time history* of the oscillations, their limiting amplitude, and the critical triggering amplitudes at which an otherwise stable motor is caused to transition to violent oscillations. Pulsing of this sort can result from random disturbances and by the passage of pieces of liner or insulation through the nozzle leading to a momentary decrease in the effective throat area. Thus, it is important to characterize this aspect of motor behavior.

As described in the last section, shock waves are a major nonlinear attribute of axial mode oscillations in solid rockets.[14,19,20,25] There is no question that shock-like features dominate the gas motions when waves grow to finite amplitude. The steepening process is a natural feature of nonlinear resonant oscillations of gas columns.[35,66] Recognition of the role played by shock waves in combustion instability is certainly not widespread, although many investigators, especially in the case of liquid engine instability have examined this possibility.[19,20,25,67] However, current liquid engine or solid rocket motor instability prediction methods do not recognize this obviously important aspect of the problem. It constitutes yet another nonlinear feature that must be accommodated if a complete theoretical foundation is to be constructed.

D. Formulating a nonlinear instability algorithm

In this section we briefly discuss what is needed from the theoretical standpoint to provide a useful analytical framework for combustion instability. It is necessary to accommodate the features we have identified as key elements for a correct physical representation. We must discard models based on the acoustic point of view. Nonlinear energy losses in steep wave fronts and energy flow to the wave structure from combustion must be accommodated. By far, the most effective method for incorporating this large array of physical/chemical interactions is by application of a global

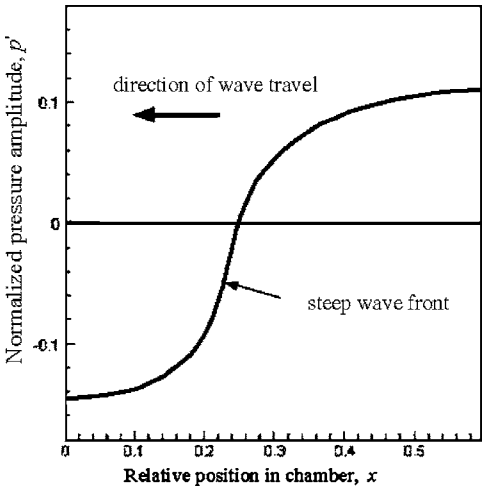

FIG. 5. Culick's fully steepened wave.

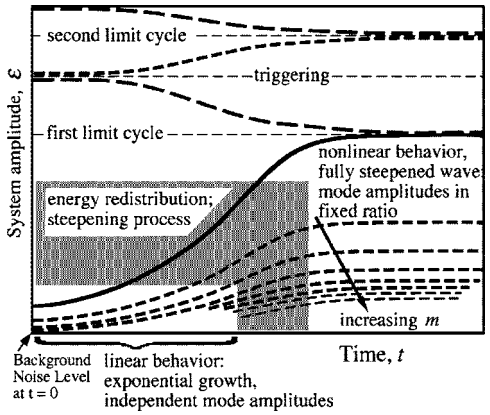

FIG. 6. Nonlinear evolution of system amplitude.

nonlinear energy balance. Methods based on the usual perturbed acoustic wave equation cannot properly account for the many interactions that must be captured.

E. Mathematical strategy

Since a central concern is the handling of steep fronted waves, it is necessary to carefully lay out a solution technique that will lead to a practical predictive algorithm. To make the mathematical problem tractable, we choose to avoid fashionable numerical strategies such as the method of characteristics or a full computational fluid dynamics (CFD) treatment of the problem. Either of these techniques would likely fail in the problem we are attempting to solve here.

What is required is an approach that bridges the gap between the earlier perturbation techniques that limit the solutions to linear gas motions and other *ad hoc* methods such as those introduced by Culick to study nonlinear features of combustion instability.[17,24] Figure 5 displays a frame from an animation of the development of the wave system with time predicted by Culick's model. At the instant shown, the wave has nearly reached its final limit condition, and the wave front is moving to the left. This wave pattern is the composite of twenty acoustic modes. Energy from the lower order modes has cascaded to the higher modes until the stationary state shown in the figure has been reached. This "mode coupling" effect clearly represents the natural steepening process. What began as a set of standing acoustic modes has transitioned into a single traveling steep-fronted wave. Once limiting has occurred, the wave simply bounces back and forth between the ends of the chamber. The period of oscillation corresponds to the first longitudinal acoustic mode. What is shown here agrees in every respect with the fully steepened condition described in earlier works.[19,20] The calculations and animation from which Fig. 5 was taken were carried out by French. He has implemented Culick's nonlinear model in the SSP. It can now be run for longitudinal modes with arbitrary chamber cross-sectional area distribution.

In the problem of central interest here, we are not concerned with the steepening process, *per se*; rather, we wish to understand the gas motions in the fully steepened state. Figure 6 illustrates several aspects of the problem we must solve.

This diagram shows in schematic form all features of combustion instability that appear experimentally. Furthermore, it provides a useful way to categorize the various analytical methods by which we attempt to understand this very complicated physical problem. Figure 6 shows that if the waves grow from noise in the linear fashion, the motion is linear and each acoustic mode grows individually according to the balance of energy gains and losses peculiar to that operating frequency. In general, the lowest order mode grows most rapidly because it requires less energy to excite. As the oscillations grow to finite amplitude, nonlinear effects appear and there is a phase in which energy is redistributed from lower to higher modal components; it is this process that is described in Culick's nonlinear model.

As the wave steepens, the relative amplitudes of the constituent acoustic modes reach a frozen state corresponding to shock-like behavior. This is the fully nonlinear state illustrated in the figure. In pulse testing of motors, the steepening process is almost instantaneous. For example, Brownlee[14] notes that when the pulse is fired, "…the injected flow disturbance traversed the length of the motor, partially reflected at the nozzle end, and became a steep-fronted shock-like wave in one cycle." Thus, in modeling such effects, it is unnecessary to trace the full steepening process. The relative wave amplitudes are readily estimated from a large database of experimental results. It is readily established that precise knowledge of the relative amplitudes is not necessary to achieve an accurate estimate of the limit cycle and triggering amplitudes.

We must formulate a mathematical strategy that yields the essential information; namely, the limit amplitude reached by the system in the fully steepened state. This is the information required by the motor designer in assessing potential vibration levels, and as we will show, the severity of heat loads and force levels on fragile injector components.

The key to simplifying the nonlinear problem is to assume that the *fully steepened traveling* wave is a composite of the chamber normal modes:

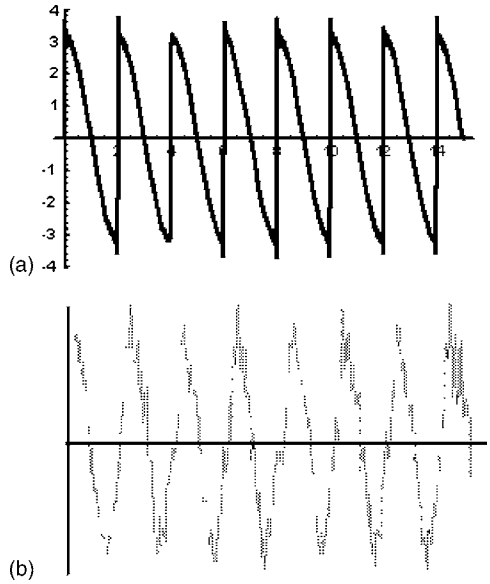

FIG. 7. Measured vs calculated waveform: (a) waveform calculated using twenty modes in Eq. (1) and (b) waveform measured experimentally in a preburner undergoing severe oscillation.

$$p(\mathbf{r},t) = \varepsilon(t)\sum_{n=1}^{\infty} A_n(t)\psi_n(\mathbf{r}), \tag{3}$$

where $\varepsilon(t)$ is the instantaneous wave amplitude, p is the oscillatory pressure, $(\mathbf{r},t)$ represent the spatial position vector and time, respectively, and n is the mode integer. This is a proven simplifying strategy[19,20] that follows directly as the final form reached in Culick's calculations. It conforms well to all experimental features that must be accommodated in our solution algorithm. Before proceeding with the analysis, let us first test this model to see if it contains the necessary features and flexibility.

F. Traveling shocked acoustic waves by superposition of standing normal modes

Equation (3) provides a useful tool and a way to avoid all computational difficulties associated with modeling of the unsteady flowfield. In the case of simple longitudinal oscillations in a chamber of constant cross section, the functions in the summation are, for example:

$$A_n(t) = \left(\frac{8n}{4n^2+1}\right)\sin\left(\frac{n\pi a_0}{L}\right),$$
$$\psi_n(r) = \cos\left(\frac{n\pi z}{L}\right), \tag{4}$$

where L is the chamber length and z is the axial position. If Eq. (3) is evaluated with these parameters, the waveform illustrated in Fig. 7(a) is produced. This should be compared to a measured waveform in Fig. 7(b). The data shown came from precision pressure measurements in a liquid rocket preburner undergoing high-amplitude nonlinear longitudinal oscillations.

It is clear that Eq. (3) yields an excellent model of the actual waveform. It can be used to represent any experimental waveform by fitting a Fourier series to the data. It is known that once the wave has reached the limit cycle conditions, the waveform remains essentially frozen; only the amplitude then changes with time. This is a powerful computational simplification.

G. Notation

The following dimensionless variables will be used (the asterisk denotes dimensional quantities; the subscript "0" indicates quiescent chamber reference conditions):

$$\begin{cases} p = p^*/P_0, \\ \rho = \rho^*/\rho_0, \\ T = T^*/T_0, \\ \mathbf{u} = \mathbf{u}^*/a_0, \\ \mathbf{r} = \mathbf{r}^*/L, \end{cases} \quad \begin{cases} \mathbf{F} = \mathbf{F}^*/(\rho_0 a_0^2/L), \\ t = t^*/(L/a_0), \\ \boldsymbol{\omega} = \boldsymbol{\omega}^*/(a_0/L), \\ e = e^*/a_0^2, \end{cases} \tag{5}$$

where $\mathbf{F}$ is a body force, (ρ,T) denote the density and temperature, respectively, $(\mathbf{u},\omega)$ are the instantaneous velocity and vorticity, respectively, and e is the specific internal energy. The dimensionless governing equations are

Continuity:

$$\frac{\partial \rho}{\partial t} + \nabla\cdot(\rho\mathbf{u}) = 0, \tag{6}$$

Momentum:

$$\rho\left(\frac{\partial \mathbf{u}}{\partial t} + \tfrac{1}{2}\nabla\,\mathbf{u}\cdot\mathbf{u} - \mathbf{u}\times\boldsymbol{\omega}\right) = -\frac{1}{\gamma}\nabla p - \delta^2\nabla\times\nabla\times\mathbf{u} + \delta_d^2\nabla(\nabla\cdot\mathbf{u}) + \mathbf{F}, \tag{7}$$

Energy:

$$\frac{\partial}{\partial t}\left[\rho\left(e+\tfrac{1}{2}\mathbf{u}\cdot\mathbf{u}\right)\right] + \nabla\cdot\left[\rho\mathbf{u}\left(e+\tfrac{1}{2}\mathbf{u}\cdot\mathbf{u}\right)\right] = \left\{\begin{array}{l} \dfrac{\delta^2}{(\gamma-1)Pr}\nabla^2 T - \dfrac{1}{\gamma}\nabla\cdot(p\mathbf{u}) + \rho\mathbf{u}\cdot(\mathbf{u}\times\boldsymbol{\omega}) \\ +\mathbf{u}\cdot\mathbf{F} + \delta^2[\boldsymbol{\omega}\cdot\boldsymbol{\omega} - \mathbf{u}\cdot(\nabla\times\boldsymbol{\omega})] \\ +\delta_d^2[(\nabla\cdot\mathbf{u})^2 + \mathbf{u}\cdot\nabla(\nabla\cdot\mathbf{u})] - \sum_{i=1}^{N} h_i^0 w_i \end{array}\right\} \tag{8}$$

Species mass fraction:

$$\rho\left[\frac{\partial Y_i}{\partial t} + \mathbf{u}\cdot\nabla Y_i\right] - \frac{\delta^2}{Pr}\nabla^2 Y_i = w_i, \tag{9}$$

State:

$$p = \rho T. \tag{10}$$

The Prandtl number Pr and viscous reference lengths (proportional to inverse square root of appropriate Reynolds numbers) appear naturally. These are defined as

$$Pr \equiv \frac{c_p \mu_0}{\kappa_0}, \quad \delta^2 = \frac{\mu_0}{a_0 \rho_0 L}, \quad \delta_d^2 = \left(\frac{\eta}{\mu} + \frac{4}{3}\right)\delta^2,$$
$$\delta_f \equiv \frac{\kappa_0}{\rho_0 c_p V_b} = \frac{\kappa_0}{\rho_0 c_p a_0 \bar{M}_b}. \tag{11}$$

The latter reference length is the reference flame length needed in regions dominated by combustion heat release. The subscript b refers to blowing conditions at the burning surface, and $(\mu_0, \kappa_0, c_p, a_0, V_b, \bar{M}_b)$ represent the dynamic viscosity, thermal conductivity, constant pressure specific heat, speed of sound, blowing velocity, and blowing Mach number, respectively. Other variables needed in modeling chemical reactions are

$$\begin{aligned} &w = w^*/(\rho_0 a_0/L)\text{: dimensionless reaction rate,} \\ &h_i^o = (h_i^o)^*/a_0^2\text{: dimensionless heat of combustion,} \\ &Y_i\text{: mass fraction for species } i. \end{aligned} \tag{12}$$

H. Separating steady and unsteady parts

The steady and unsteady parts of the variables are decomposed in the standard manner by writing

$$\rho = \bar{\rho} + \rho^{(1)}, \quad p = \bar{P} + p^{(1)}, \quad T = \bar{T} + T^{(1)},$$
$$\mathbf{u} = \bar{M}_b \mathbf{U} + \mathbf{u}^{(1)}, \quad \boldsymbol{\omega} = \bar{M}_b \nabla \times \mathbf{U} + \nabla \times \mathbf{u}^{(1)} = \bar{M}_b \boldsymbol{\Omega} + \boldsymbol{\omega}^{(1)}, \tag{13}$$

where the superscript "(1)" denotes first-order accuracy in the wave number. Since the energy balance is the key to understanding the system behavior, let us carefully work with it. In what follows, we will avoid the common simplifying assumptions such as the isentropic flow limitation. We will also carefully include heat transfer and viscosity so that, in effect, we are modeling a wave system composed of superimposed waves of compressibility, vorticity, and entropy.

Define the system energy density as

$$\mathcal{E} \equiv \rho\left(e + \tfrac{1}{2}\mathbf{u}\cdot\mathbf{u}\right). \tag{14}$$

For a calorically perfect gas the energy equation then becomes

$$\frac{\partial \mathcal{E}}{\partial t} = -\nabla \cdot \left[\rho \mathbf{u}\left(\frac{T}{\gamma(\gamma-1)} + \tfrac{1}{2}\mathbf{u}\cdot\mathbf{u}\right)\right] + \left\{\begin{aligned} &-\frac{1}{\gamma}\nabla\cdot(p\mathbf{u}) + \rho\mathbf{u}\cdot(\mathbf{u}\times\boldsymbol{\omega}) \\ &+ \delta^2[\boldsymbol{\omega}\cdot\boldsymbol{\omega} - \mathbf{u}\cdot(\nabla\times\boldsymbol{\omega})] + \delta_d^2[\mathbf{u}\cdot\nabla(\nabla\cdot\mathbf{u})] + \mathbf{u}\cdot\mathbf{F} \end{aligned}\right\} \tag{15}$$

where a shorthand notation has been adopted for the heat release in combustion processes. The body force $\mathbf{F}$ is a placeholder for two-phase flow effects such as particle damping. Note that the compressive viscous force and conduction heat transfer terms are retained. These are the source of the important nonlinear energy loss in steep wave fronts.

Using Eq. (13), one can now expand Eq. (15) to give the equation for the system amplitude. To accomplish this, the time-averaged Eq. (15) can be written as

$$2\varepsilon\frac{d\varepsilon}{dt}\langle\mathcal{E}_2\rangle = \left\langle\begin{aligned} &-\nabla\cdot\left\{\rho\mathbf{u}\left[\frac{T}{\gamma(\gamma-1)} + \tfrac{1}{2}\mathbf{u}\cdot\mathbf{u}\right]\right\} - \frac{1}{\gamma}\nabla\cdot(p\mathbf{u}) + \rho\mathbf{u}\cdot(\mathbf{u}\times\boldsymbol{\omega}) \\ &+ \mathbf{u}\cdot\mathbf{F} + \delta^2[\boldsymbol{\omega}\cdot\boldsymbol{\omega} - \mathbf{u}\cdot(\nabla\times\boldsymbol{\omega})] + \delta_d^2\mathbf{u}\cdot\nabla(\nabla\cdot\mathbf{u}) + \frac{\delta^2}{(\gamma-1)Pr}\nabla^2 T + \delta_d^2(\nabla\cdot\mathbf{u})^2 \end{aligned}\right\rangle \tag{16}$$

where

$$\langle\mathcal{E}_2\rangle = \frac{1}{\gamma\bar{P}}\left\langle\left(\frac{p'}{\gamma}\right)^2\right\rangle + \tfrac{1}{2}\bar{\rho}\langle\mathbf{u}'\cdot\mathbf{u}'\rangle \tag{17}$$

is the time-averaged oscillatory energy. Note that this consists of a "potential" energy proportional to the pressure fluctuation and a kinetic part proportional to the square of the particle velocity. The latter is not the simple acoustic particle velocity; it is the composite of the irrotational and rotational parts needed to satisfy correct boundary conditions at the chamber surfaces.

Equation (17) is similar to the familiar Kirchoff[68] reference energy density from classical acoustics:

$$\mathcal{E}_{\text{Kirchoff}} = \tfrac{1}{2}[p^{(1)}/\gamma]^2 + \tfrac{1}{2}\bar{\rho}\mathbf{u}^{(1)}\cdot\mathbf{u}^{(1)}. \tag{18}$$

The differences are largely the result of relaxing the isentropic flow assumption used in deriving Eq. (16).

I. Spatial averaging

In order to account for the net behavior of the entire system, it is now required to integrate the time-averaged

energy density over the chamber control volume. We define the reference system energy as

$$E^2 \equiv \int_V \int \int \langle \mathcal{E}_2 \rangle \mathrm{d}V = \int_V \int \int \left\langle \frac{1}{\gamma \bar{P}} \left(\frac{p'}{\bar{\gamma}} \right)^2 + \tfrac{1}{2} \bar{P} \mathbf{u}' \cdot \mathbf{u}' \right\rangle \mathrm{d}V, \tag{19}$$

where primed variables are defined by factoring out the slowly changing amplitude. For example,

$$p^{(1)} = \varepsilon(t) p'.$$

The rate of change of system amplitude can then be written in the convenient form:

$$\frac{\mathrm{d}\epsilon}{\mathrm{d}t} = \alpha^{(1)} \epsilon + \alpha^{(2)} \epsilon^2 + \alpha^{(3)} \epsilon^3 + \cdots, \tag{20}$$

where $\alpha^{(1)}$ is the linear growth rate for the composite wave system. The reader should also notice the similarity of this expression to Jensen and Beckstead's *Pi theorem* described in the last section. This expression emphasizes the fact that the nonlinear model is only as good as the linear representation of the system.

In many ways, achieving a valid linear model is the most difficult part of the entire combustion instability problem. It has in fact been the downfall of numerous past attempts. Much time and energy has been expended on attempts to correct deficiencies in the linear model by introduction of *ad hoc* fixes that are often based on guesswork, misinterpretation, and distortion of experimental evidence. The roadway is strewn with the wreckage of such attempts. We avoid the temptation to dwell on the past. Clearly, the path to success is to avoid losing any of the crucial physical information that has been collected in the system energy balance constructed here.

J. Linear growth rate

The linear part of Eq. (17) becomes

$$\alpha^{(1)} = \frac{1}{2E^2} \left\{ -\frac{1}{\gamma} \int_S \int \mathbf{n} \cdot \left[\langle p' \mathbf{u}' \rangle + \frac{\bar{M}_b \mathbf{U}}{\gamma^2 \bar{P}} \langle p'^2 \rangle \right] \mathrm{d}S - \bar{M}_b \bar{P} \int_S \int \mathbf{n} \cdot \left\langle \tfrac{1}{2} \mathbf{U} (\mathbf{u}' \cdot \mathbf{u}') + \mathbf{u}' (\mathbf{U} \cdot \mathbf{u}') \right\rangle \mathrm{d}S \right.$$
$$+ \bar{M}_b \bar{P} \int_V \int \int [\mathbf{U} \cdot \langle \mathbf{u}' \times \boldsymbol{\omega}' \rangle + \langle \mathbf{u}' \cdot (\mathbf{U} \times \boldsymbol{\omega}') \rangle + \langle \mathbf{u}' \cdot (\mathbf{u}' \times \boldsymbol{\Omega}) \rangle] \mathrm{d}V + \delta^2 \int_S \int \mathbf{n} \cdot \langle \mathbf{u}' \times \boldsymbol{\omega}' \rangle \mathrm{d}S$$
$$\left. + \delta_d^2 \int_V \int \int \langle \mathbf{u}' \cdot \nabla (\nabla \cdot \mathbf{u}') \rangle \mathrm{d}V + \int_V \int \int \langle \mathbf{F} \rangle \mathrm{d}V \right\}, \tag{21}$$

where only the placeholders for combustion heat release and two-phase flow interactions are shown. Please note that we have not assumed that the mean pressure is constant, as is usually done. The quasi-steady chamber pressure, $\bar{P}$, is a slowly changing parameter that is clearly linked to the growth of the waves. In order to evaluate the linear system stability, one must know $\bar{P}$, which, as it happens, is an important link to the mean (DC) pressure shift.

Careful evaluation of the volume integrals in Eq. (21) leads to the vanishing of several of the terms shown. One of these is the Culick flow turning effect, which has been the source of considerable controversy in the solid propellant rocket instability research community.[42,47,69] Unfortunately, this term leads to a damping effect, which in many motor evaluations is as large as other main contributions to the energy balance. To illustrate the handling of its source in Eq. (21), we now examine the specific term from which flow turning originates:

$$\alpha_4^{(1)} = \frac{\bar{M}_b \bar{P}}{2E^2} \int_V \int \int (\mathbf{U} \cdot \langle \mathbf{u}' \times \boldsymbol{\omega}' \rangle + \langle \mathbf{u}' \cdot \mathbf{U} \times \boldsymbol{\omega}' \rangle) \mathrm{d}V. \tag{22}$$

The subscript "4" is an artifact of the numbering system introduced by Flandro and Majdalani[43] and later used by Majdalani, Flandro, and Fischbach[55] to keep track of the many linear stability contributions in Eq. (21). Flow turning was first identified by Culick[3,9] in his one-dimensional calculations as a result of forcing satisfaction of the no-slip condition (which could not be accomplished in his three-dimensional model because of the irrotational flow assump-

tion). Flandro[42,43,47] later showed that the actual source of the flow turning was the irrotational part of the second term in Eq. (22). None of the earlier stability calculations incorporated all of the rotational terms represented in Eq. (22). These appear because we have now used the complete energy balance equation. When *all* of the terms are properly accounted for, then application of the familiar scalar triple product identity

$$\mathbf{A}\cdot(\mathbf{B}\times\mathbf{C})=\mathbf{B}\cdot(\mathbf{C}\times\mathbf{A})$$

leads to

$$\mathbf{U}\cdot\langle\mathbf{u}'\times\boldsymbol{\omega}'\rangle+\langle\mathbf{u}'\cdot\mathbf{U}\times\boldsymbol{\omega}'\rangle=\langle-\mathbf{u}'\cdot\mathbf{U}\times\boldsymbol{\omega}'\rangle+\langle\mathbf{u}'\cdot\mathbf{U}\times\boldsymbol{\omega}'\rangle=0. \tag{23}$$

Flow turning has now vanished. This result agrees with considerable experimental evidence and with other analyses.[70,71]

This correction to the linear growth rate leads to major improvements in correspondence with experimental data. The lesson here is that only by accounting for *all* unsteady energy gains and losses can a correct linear stability theory be constructed. Other terms in Eq. (21) once thought to have important stability implications do not appear when the integrals are carefully evaluated.

K. Linear driving mechanisms

Equation (21) reflects all potentially important linear sources of unsteady energy as well as damping effects. Many years of experience have shown that the first pair of terms represented by the surface integral

$$\alpha_1^{(1)}=-\frac{1}{2\gamma E^2}\int\int_S\left(\langle p'\mathbf{n}\cdot\hat{\mathbf{u}}\rangle+\frac{\bar{M}_b}{\gamma^2\bar{P}}\mathbf{n}\cdot\mathbf{U}\langle p'^2\rangle\right)\mathrm{d}S \tag{24}$$

play a central role in driving acoustic waves. They are also the origin of the important nozzle damping effect. In recent investigations of the thermoacoustic energy conversion process in Rijke tubes, Majdalani, Entezam, and Van Moorhem[72–74] have identified the first term $\langle p'\mathbf{n}\cdot\hat{\mathbf{u}}\rangle$ to be the primary agent responsible for driving the Rijke-type oscillations. These studies have been corroborated using experimental, CFD, and analytical scaling techniques. In cases in which the combustion energy release occurs close to the surface (as in a burning solid propellant) or near the injector surface (in liquid rockets), this term is the primary source of unsteady energy. At first glance, it appears that Eq. (21) should represent zero contribution since for acoustic motions the pressure and velocity fluctuations are 90° out of phase. However, one must account for the phase shift in the combustion zone region of nonuniformity. This is done in the solid propellant case by introducing the admittance function accounting for myriad chemical and physical processes within the flame zone. For example, one defines

$$\mathbf{n}\cdot\hat{\mathbf{u}}=-\bar{M}_bA_b^{(r)}\frac{p'}{\gamma} \tag{25}$$

expressing the normal velocity fluctuation in terms of the pressure disturbance that creates it. Major effort is expended in the solid rocket community in characterizing the admittance function. This is a familiar scenario and need not be reviewed in depth. The solid rocket literature is replete with discussion of this important concept. A lucid treatment is carried out by Culick and Yang.[6] The associated nozzle damping is also described in detail in this and many other documents.

The first term in Eq. (21) is also a potent source of energy in liquid rocket instability analysis. If $\langle p'\mathbf{n}\cdot\hat{\mathbf{u}}\rangle$ is evaluated at the injection surface accounting for the phase difference between fluctuations in the incoming oxidizer and fuel velocities and the pressure oscillations at the interface, it will be seen that a powerful analog to the solid rocket pressure coupling is identified. Examination of experimental data shows that indeed the pressures in the oxidizer and fuel feed lines upstream of the injector reflect the pressure fluctuations in the chamber and exhibit the phase differences needed to explain this powerful unsteady energy source. Additional energy is supplied to the waves via the more traditional distributed combustion. However, there can be no doubt that any energy source located at a pressure antinode (e.g., the injector surface) is a potent driver of oscillations of the type observed. These matters are currently undergoing thorough study by the authors.

L. Effects of nonlinearity

It is now required to examine nonlinear terms arising from the expansion of Eq. (13). The most important of these are the energy losses incurred in steep wave fronts. Let us focus on the last set of terms in Eq. (16). After temporal and spatial averaging, we are left with

$$\int\int\int_V\left\langle\frac{\delta^2}{(\gamma-1)Pr}\nabla^2T+\delta_d^2(\boldsymbol{\nabla}\cdot\mathbf{u})^2\right\rangle\mathrm{d}V. \tag{26}$$

Those readers with training in gas dynamics will recognize in this term the source of the entropy gain and associated energy loss in a steep wave front. In fact, this term is usually ignored because it is only significant if there are very steep gradients in particle velocity and temperature. Let us evaluate this term by considering a very small portion of the chamber volume that encompasses the shock layer formed by a steepened wave system. The shock layer can be treated as a region of nonuniformity as illustrated in Fig. 8.

Following standard procedures, Eq. (26) can be reduced to the classical textbook result showing the origin of the entropy gain in the shock wave. By manipulations using the Rankine-Hugoniot equations, we find the formula for the energy loss in the steep wave to be

$$\left(\frac{\mathrm{d}E}{\mathrm{d}t}\right)_{\text{shock}}=-\frac{S_{\text{port}}}{\gamma(\gamma-1)}\frac{(s_2-s_1)^*}{c_v}=-\left(\frac{\epsilon_{\text{shock}}}{\bar{P}}\right)^3S_{\text{port}}\left(\frac{\gamma+1}{12\gamma^3}\right) \tag{27}$$

leading to a simple approximation for the nonlinear stability parameter in Eq. (17); namely,

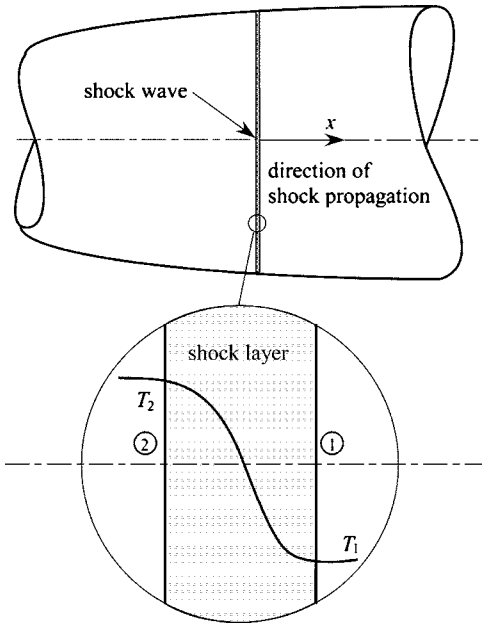

FIG. 8. Shock layer structure.

$$\alpha^{(2)} = -\frac{(\gamma+1)}{3E^2}\left(\frac{\xi}{2\gamma}\right)^3 S_{\text{port}}, \tag{28}$$

where ξ is a factor dependent upon the assumed waveform for the traveling shock wave, and S_{port} is the area of the shock front. In the longitudinal case, this is simply the cross-sectional area of the duct at a convenient location.

This nonlinear loss effect is the principal damping mechanism in both liquid and solid propellant motors, and is the key element in understanding the limit cycle behavior so often encountered when finite amplitude waves appear. It is tempting to carry the implied perturbation series in Eq. (20) to higher than second order in the system amplitude. However, such an extension is not justified in the present situation because we assume that the unsteady flowfield and mode shape information for the chamber are accurate only to the first order in wave amplitude. Let us now test the results that we have found against experimental evidence.

M. Limit cycle amplitude

In solid propellant rockets, one is seldom interested in tracing the details of the growth of the waves to their final state. Such motors usually operate for very long time on the time scale of the wave motions with very slow changes in the steady operating parameters. For this reason, strictly linear models provide little useful information in the predictive sense. There is, however, a well-known rule of thumb that suggests that large values of the linear growth rate $\alpha^{(1)}$, estimated, for example, by using Eq. (21), correlate with large values of the limit cycle amplitude. Clearly, it is the latter amplitude that is of concern, since it is a measure of the vibration and other impacts on the system due to the oscillations.

What is required is information concerning the limit amplitude reached as the wave system approaches a fully steepened form. Equation (20) provides the required limit amplitude. In the fully steepened state, the wave amplitude is stationary, and it is readily seen that the limit amplitude is

$$\epsilon_{\text{limit}} = -\frac{\alpha^{(1)}}{\alpha^{(2)}}, \tag{29}$$

which is physically meaningful only when $\alpha^{(2)}$ is negative. This will always be the case for the shock loss mechanism described by Eq. (27). To the knowledge of the authors, there has never been either experimental or theoretical evidence of second-order interactions that are not damping effects. However, there may be nonlinear driving mechanisms of this sort yet to be discovered. Equation (29) has been tested for many solid rocket data sets and has been found to yield an excellent estimate of the limit amplitude. Again, note that good results depend critically on a valid linear stability estimate.

N. Triggering amplitude

This is a controversial subject. If one examines Fig. 6 in the context of Eq. (20) (extended to higher orders in the wave amplitude), it is apparent that it is theoretically possible to raise the amplitude of a system oscillating in its lowest limit cycle to a yet higher limit amplitude by adding sufficient energy in a pulse to raise the oscillations above a critical triggering level. This is what might be termed *true triggering*. Careful examination of solid rocket data has made it clear that this scenario seldom fits what is actually observed. In every case studied by the authors, motors that exhibited "triggering" were *linearly unstable* motors. That is, they are not stable motors that are *triggered* into a high-amplitude limit cycle. When such burners operate without deliberate pulsing, the wave system grows so slowly from the always-present random noise, that oscillations are barely measurable by the end of the burn. However, when the motor is disturbed by a sufficiently large pulse, the broadband energy increment can excite finite amplitude steep-fronted waves. The system then grows rapidly to the limit cycle amplitude. Calculations using Eq. (20) agree very well with actual observations. We believe that true triggering is seldom, if ever, observed in actual rocket motors. Much of the confusion over this issue has resulted from application of faulty predictive codes that almost always predict a linearly stable system. A classic example can be found in the Blomshield data.[37] Every motor fired in this test series was predicted by the SSP to be linearly stable. In fact, there is no doubt that many of the motors were linearly unstable at least during part of the burn. Unless pulsed, only very low level oscillations were present. Sufficiently strong pulsing during linearly unstable operation led to violent oscillations in several tests.

IV. THE DC PRESSURE SHIFT

The mean pressure rise, or DC shift, is an oft-observed feature of nonlinear instability. As illustrated in Fig. 3, it is closely linked to the growth and limiting of the system of acoustic waves. A test of the validity of the theory presented in this paper is its ability to predict this classical feature of combustion instability. What we will demonstrate here is that

the same mechanism that drives the oscillations [first term in Eq. (21)] is also the source of the DC shift phenomenon.

Until now, explaining the mean pressure excursion has required invoking *ad hoc* flow reversal, *velocity coupling*, burning surface velocity rectification, or "acoustic erosivity" effects.[25] These confusing and often simply misleading paraphernalia can now be discarded.

Clearly, any attempt to understand one nonlinear feature without due attention to other closely connected features does not take full advantage of the experimental data. In this section, we demonstrate the benefits of accommodating all of the key observations in formulating the mathematical approach.

Previous theoretical models have been based on the assumption that the mean gas properties remain constant. For example, Culick and Yang[6] write, "…we assume that the average values do not vary with time. That is not an essential assumption, but to correct it requires considerable elaboration not justified here. However, there are practical situations in which changes in the average values, particularly the pressure, are important. No thorough analysis of such cases has been given." In what follows we present the missing analysis.

The formulation described in the last section has been deliberately written without the assumption of constant mean properties. Thus, we are able to study the coupling between the unsteady and *quasisteady* gas motions. It is assumed that the chamber mean temperature is controlled by combustion heat release and is therefore essentially constant. Thus, the state equation shows that mean pressure and density are slowly changing functions of time. The surface reference Mach number and the wave amplitude are also slow functions of time as already demonstrated.

A. Formula for rate of change of mean pressure

The source of the DC shift is readily found if nonlinear terms are retained in the continuity equation. Expanding Eq. (6) and taking the time average yields

$$\frac{d\bar{P}}{dt} = -\nabla \cdot (\bar{M}_b \bar{\rho} \mathbf{U}) - \frac{\varepsilon^2}{\gamma} \nabla \cdot \langle p^{(1)} \mathbf{u}^{(1)} \rangle, \tag{30}$$

where the first term on the right represents quasisteady mass flux at the chamber boundaries due to combustion and nozzle outflow. The similarity of the second term to the pressure-coupled acoustic driving in Eq. (21) is intriguing. Integration over the chamber volume leads to the equation for the rate of change of the quasisteady chamber operating pressure:

$$\frac{d\bar{P}}{dt} = \left\{ -\frac{1}{\bar{V}} \int_S \int \mathbf{n} \cdot (\bar{\rho} \bar{M}_b \mathbf{U}) dS - \varepsilon^2 \left(\frac{1}{\gamma \bar{V}} \right) \int_S \int \mathbf{n} \cdot \langle p^{(1)} \mathbf{u}^{(1)} \rangle dS \right\}. \tag{31}$$

The first term is handled by means of the standard steady internal ballistics calculations; the second leads to the mean pressure shift. Notice that it is proportional to the second order of the wave amplitude. Equation (31) verifies the anticipated close coupling between the mean pressure rise and the growth and limiting of the pressure oscillations.

B. Simulating and predicting motor behavior

The results for the nonlinear system growth and the corresponding mean pressure excursion must be computed simultaneously. When the several system models are collected and the integrals are performed, we are left with a pair of coupled nonlinear, ordinary differential equations:

$$\frac{d\varepsilon}{dt} = \alpha^{(1)} \varepsilon + \alpha^{(2)} \varepsilon^2 + \cdots,$$
$$\frac{d\bar{P}}{dt} = \beta^{(1)} + \beta^{(1)} \varepsilon^2. \tag{32}$$

These are readily solved using a simple numerical algorithm. The result is the time history of the growth and limiting of the pressure oscillation amplitude and the accompanying growth and limiting of the mean pressure amplitude. These results agree in every way with actual motor data.

C. Results

The methods described here are being used to enhance the SSP by enabling the motor analyst/designer to predict the stability of a given system and to diagnose sets of experimental data.

We show here some preliminary results from application of Eq. (32) in the difficult dilemma represented by Blomshield's data set.[33,37,75] In virtually all of his motor configurations, the SSP code predicted stable behavior (see Fig. 4). Yet, many of the motors were readily pulsed into high-amplitude oscillations. We seek here to understand this triggering phenomenon. Numerical solutions of Eq. (32) yield the required information.

Figure 9(a) shows a pressure versus time trace for a cylindrical motor from this test series. The progressive pressure rise results from the increasing burning surface area with time. The mean pressure shift and pressure oscillations are clearly shown. Data came from a pressure transducer at the motor forward end. The spectrum was dominated by the 1L (first longitudinal mode) accompanied by a great many harmonics representing strong evidence for steep-fronted waves. Figure 9(b) shows the predicted behavior of this motor found by solving Eq. (32) using geometrical and physical data from the tests; no curve fitting was employed.

All important features of the actual data are well represented. Notice that even though the system is linearly unstable, no wave growth or DC shift occurs unless the motor is pulsed. Examination of the numerical results reveals that this motor was marginally stable during the first part of the burn, but the net linear growth rate became positive after about $t=0.5$ s. The motor was then susceptible to pulsing, and could be "triggered" into violent oscillations. Parametric studies have shown that the predicted DC shift and corresponding oscillation limit cycle amplitude are insensitive to the pulse amplitude; this agrees with experimental findings.

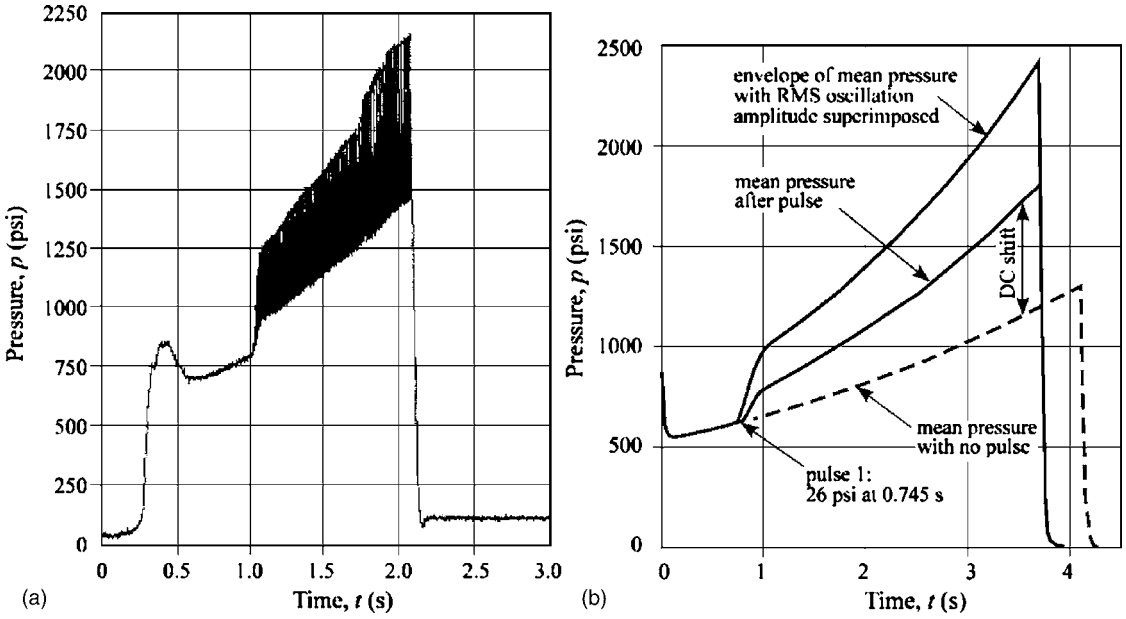

FIG. 9. Measured (a) and simulated (b) pressure vs time for motor No. 9 [Blomshield (37)].

Similar comparisons of predicted and measured behavior are shown in Figs. 10 and 11 for the other two cylindrical motors (Nos. 10 and 13) fired in this test series. Motor 10 follows closely the pattern that was predicted for Motor 9. Both of these were full-length motors with fundamental oscillation frequency of about 300 Hz. Motor 13 was a half-length motor with otherwise similar geometry.

Motors 11 and 13 had nozzles sized to yield an average operating pressure of 500 psi; Motor 9 was intended to operate at about 1000 psi. All motors described here were predicted to be stable throughout the firing by the SSP. Again, we see evidence of the failure of this analytical tool.

Note that in both full length motors our new predictive computer code has captured the main features shown in the experimental data.

In the half-length Motor 13, we see some interesting results. This motor was pulsed three times and did not exhibit the violent oscillations observed in the other two tests. However, careful inspection of the data reveals that oscillations were indeed present despite the prediction from the SSP code that Motor 13 was a stable motor. Since a large DC shift did not appear, the investigator[37] presumed that this was indeed a stable firing in agreement with the SSP prediction. If the reader will examine the last part of the pressure time trace, evidence of a DC shift is clearly present. It apparently grew without a pulse from pressure oscillations already in the system.

For Motor 13, the new predictive algorithm yields a result that is in good agreement with the measurements. No violent DC pressure rise was predicted, but, again, a small

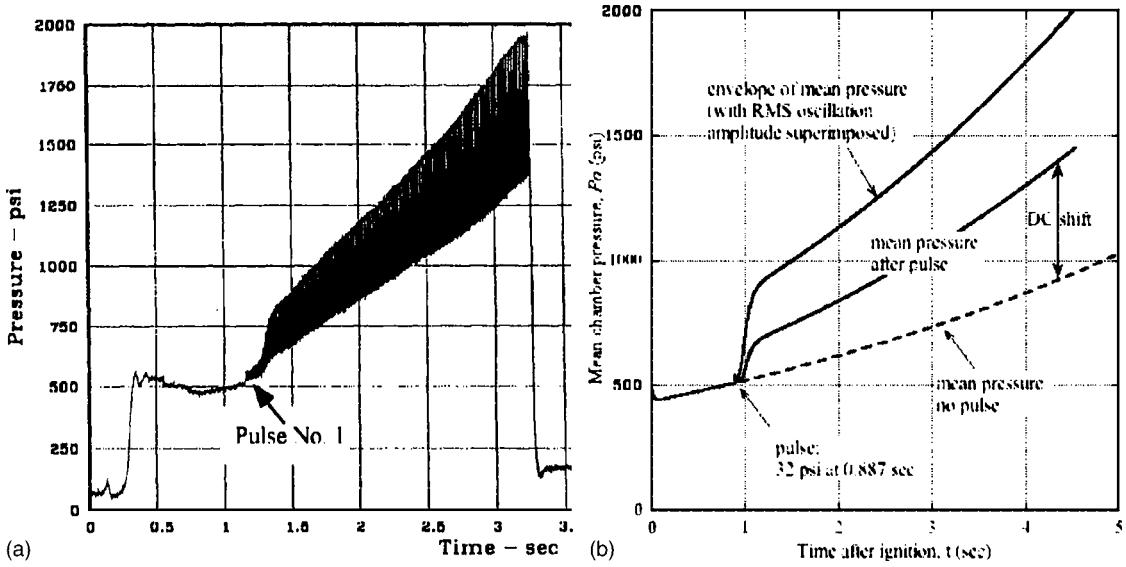

FIG. 10. Same comparison for Motor No. 10.

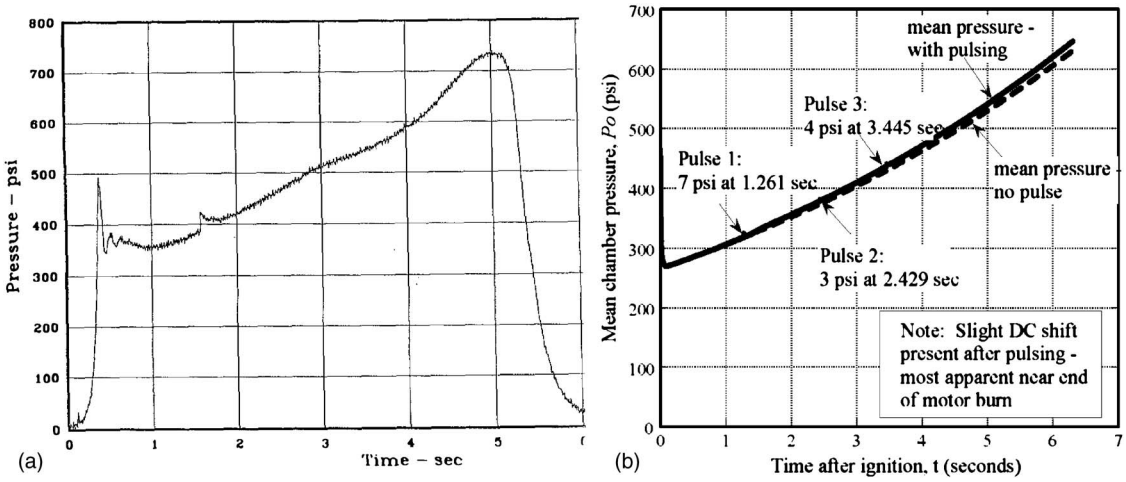

FIG. 11. Same comparison for Motor No. 13.

elevation was present as in the experimental data. We must conclude that Motor 13 was indeed unstable! The main reason for the less violent oscillations was the reduced propellant surface area in the half-length grain. The primary energy source for both the oscillations and the DC pressure rise was thereby much reduced. Thus, on the basis of a limited number of test cases we feel that the basic validity of our approach has been demonstrated.

To summarize: we have devised a new procedure for estimating the tendency for a given rocket motor chamber to exhibit nonlinear combustion instability. The new algorithm gives not only growth rate information and the associated stability maps, but more importantly predicts the evolution of the system oscillation amplitude and the mean pressure shift. These analytical/numerical tools promise to give the motor designer the ability to avoid design features that may promote combustion instability much earlier in the development cycle than possible using other methods.

If combustion instability problems are encountered in the motor test phase of development, these new tools yield an improved method for correlating experimental data and correctly interpreting the results. They also provide the ability to test and perfect corrective mechanisms if these become necessary.

V. CONCLUSIONS

In this paper we have demonstrated a predictive algorithm based on sound theoretical foundations that fully explains the nonlinear behavior observed in unstable rocket motor systems. The close connection between pressure coupling, the main linear driving mechanism in combustion instability, and the DC pressure shift has been illuminated. Knowledge of the physical parameters that control the pressure coupling, namely, the admittance function or response function of the propellant, makes it possible to determine the growth and limiting amplitude of both the wave system and the accompanying mean pressure shift. Much work is left in perfecting and fine tuning the new methodology. Eventually, these tools will be incorporated into commercially available analysis tools that will enable the rocket motor designer and experimentalist to better deal with combustion instability problems.

ACKNOWLEDGMENTS

This work was sponsored partly by the University of Tennessee Space Institute, partly by Software and Engineering Associates, Inc. (SEA), Carson City, NV, and partly, by the National Science Foundation (NSF). The first author wishes to express appreciation for additional support from the Edward J. and Carolyn P. Boling Chair of Excellence in Advanced Propulsion, University of Tennessee. The second and third authors are deeply grateful for the support received from NSF Grant No. CMS-0353518. The authors are also grateful for the assistance and feedback received from Dr. Jonathan C. French, Senior Research Engineer, SEA.

[1] S. I. Cheng, "High frequency combustion instability in solid propellant rockets: Part I," Jet Propul. **24**, 27 (1954); "High frequency combustion instability in solid propellant rockets: Part II," Jet Propul. **24**, 102 (1954).
[2] F. E. C. Culick, "Acoustic oscillations in solid propellant rocket chambers," Acta Astron. **12**, 113 (1966).
[3] F. E. C. Culick, "The stability of one-dimensional motions in a rocket motor," Combust. Sci. Technol. **7**, 165 (1973).
[4] F. E. C. Culick, "Stability of three-dimensional motions in a rocket motor," Combust. Sci. Technol. **10**, 109 (1974).
[5] F. E. C. Culick, "Nonlinear behavior acoustic waves in combustion chambers, parts 1 and 2," Acta Astronaut. **3**, 714 (1976).
[6] F. E. C. Culick and V. Yang, "Prediction of the stability of unsteady motions in solid propellant rocket motors," in *Nonsteady Burning and Combustion Stability of Solid Propellants*, edited by L. De Luca, E. W. Price, and M. Summerfield, AIAA Progress in Astronautics and Aeronautics Vol. 143 (AIAA, Washington, DC, 1992), pp. 719–779.
[7] R. W. Hart and F. T. McClure, "Combustion instability: Acoustic interaction with a burning propellant surface," J. Chem. Phys. **10**, 1501 (1959).
[8] R. W. Hart and F. T. McClure, "Theory of acoustic instability in solid propellant rocket combustion," Tenth Symposium (International) on Combustion, University of Cambridge, Cambridge, England, 17–21 August, 1047–1066 (1964).
[9] F. E. C. Culick, "Stability of longitudinal oscillations with pressure and velocity coupling in a solid propellant rocket," Combust. Sci. Technol. **2**, 179 (1970).

[10]F. E. C. Culick, "Combustion instabilities in propulsion systems," *Combustion Instabilities Driven by Thermo-Chemical Acoustic Sources*, American Society of Mechanical Engineers, NCA 4, HTD 128, New York, 33 (1989).
[11]F. E. C. Culick, "Combustion instabilities in propulsion systems," in *Unsteady Combustion* (Kluwer Academic, Dordrecht, 1996), pp. 173–241.
[12]E. W. Price and J. W. Sofferis, "Combustion instability in solid propellant rocket motors," Jet Propul. **28**, 190 (1958).
[13]V. Yang, J. Wicker, and M. W. Yoon, "Acoustic waves in combustion chambers," in *Liquid Rocket Engine Combustion Instability*, edited by V. Yang and W. E. Anderson, AIAA Progress in Astronautics and Aeronautics Vol. 169 (AIAA, Reston, VA, 1995), pp. 357–376.
[14]W. G. Brownlee, "Nonlinear axial combustion instability in solid propellant motors," AIAA J. **2**, 275 (1964).
[15]W. G. Brownlee, "An experimental investigation of unstable combustion in solid propellant rocket motors," Ph.D. dissertation, California Institute of Technology, 1959.
[16]L. Green, Jr., "Observations on the irregular reaction of solid propellant charges," Jet Propul. **26**, 655 (1956).
[17]F. E. C. Culick, "Non-linear growth and limiting amplitude of acoustic oscillations in combustion chambers," Combust. Sci. Technol. **3**, 1 (1971).
[18]F. E. C. Culick, "Combustion instabilities: mating dance of chemical, combustion, and combustor dynamics," AIAA Paper 2000-3178, Huntsville, AL, 2000. 36th AIAA/ASME/SAE/ASEE Joint Propulsion Conference and Exhibit, 16–19 July.
[19]G. A. Flandro, "Approximate analysis of nonlinear instability with shock waves," AIAA Paper 82-1220, Cleveland, OH, 1982. 18th AIAA/SAE/ASME Joint Propulsion Conference, 21–23 June.
[20]G. A. Flandro, "Energy balance analysis of nonlinear combustion instability," J. Propul. Power **1**, 210 (1985).
[21]G. A. Flandro, "Analysis of nonlinear combustion instability," SIAM Minisymposium, York, UK, 1998.
[22]V. Yang, S. I. Kim, and F. E. C. Culick, "Triggering of longitudinal pressure oscillations in combustion chambers, I: Nonlinear gasdynamics," Combust. Sci. Technol. **72**, 183 (1990).
[23]F. E. C. Culick, "Some recent results for nonlinear acoustics in combustion chambers," AIAA J. **32**, 146 (1994).
[24]F. E. C. Culick, V. S. Burnley, and G. Swenson, "Pulsed instabilities in solid-propellant rockets," J. Propul. Power **11**, 657 (1995).
[25]J. N. Levine and J. D. Baum, "A numerical study of nonlinear instability phenomena in solid rocket motors," AIAA J. **21**, 557 (1983).
[26]W. G. Brownlee, "Shock propagation is solid-propellant rocket combustors," AIAA J. **4**, 1132 (1966).
[27]S. Malhotra and G. A. Flandro, "On the origin of the DC shift," AIAA Paper 97-3249, Seattle, WA, 1997. 33rd AIAA/ASME/SAE/ASEE Joint Propulsion Conference and Exhibit, 6–9 July.
[28]E. W. Price, "Experimental observations of combustion instability," in *Fundamentals of Solid-Propellant Combustion*, edited by K. Kuo and M. Summerfield, AIAA Progress in Astronautics and Aeronautics Vol. 90 (AIAA, New York, 1984), pp. 733–790.
[29]G. A. Flandro, J. Majdalani, and J. C. French, "Incorporation of nonlinear capabilities in the standard stability prediction program," AIAA Paper 2004-4182, Fort Lauderdale, FL, 2004. 40th AIAA/ASME/SAE/ASEE Joint Propulsion Conference and Exhibit, 11–14 July.
[30]G. A. Flandro, J. Majdalani, and J. D. Sims, "Nonlinear longitudinal mode instability in liquid propellant rocket engine preburners," AIAA Paper 2004-4162, Fort Lauderdale, Florida, 2004. 40th AIAA/ASME/SAE/ASEE Joint Propulsion Conference and Exhibit, 11–14 July.
[31]G. A. Flandro, J. Majdalani, and J. D. Sims, "On nonlinear combustion instability in liquid propellant rocket engines," AIAA Paper 2004-3516, Fort Lauderdale, FL, 2004. 40th AIAA/ASME/SAE/ASEE Joint Propulsion Conference and Exhibit, 11–14 July.
[32]F. S. Blomshield, J. E. Crump, H. B. Mathes, R. A. Stalnaker, and M. W. Beckstead, "Stability testing of full-scale tactical motors," J. Propul. Power **13**, 349 (1997).
[33]F. S. Blomshield, H. B. Mathes, J. E. Crump, C. A. Beiter, and M. W. Beckstead, "Nonlinear stability testing of full-scale tactical motors," J. Propul. Power **13**, 356 (1997).
[34]R. C. Jensen and M. W. Beckstead, "Limiting amplitude analysis," Technical Report., Hercules Incorporated, Magna, Utah, 1973.
[35]R. A. Saenger and G. E. Hudson, "Periodic shock waves in resonating gas columns," J. Acoust. Soc. Am. **32**, 961 (1960).
[36]W. G. Brownlee and F. E. Marble, "An experimental investigation of unstable combustion in solid propellant rocket motors," in *ARS Progress in Astronautics and Rocketry: Solid Propellant Research*, edited by M. Summerfield (Academic, New York, 1960), Vol. 1, pp. 455–494.
[37]F. S. Blomshield, "Stability testing and pulsing of full scale tactical motors, parts I and II," Naval Air Warfare Center, Technical Report, NAWCWPNS TP 8060, February 1996.
[38]J. G. Sotter, J. W. Woodward, and R. M. Clayton, "Injector response to strong high-frequency pressure oscillations," J. Spacecr. Rockets **6**, 504 (1969).
[39]J. G. Sotter and R. M. Clayton, "Monitoring the combustion process in large engines," J. Spacecr. Rockets **4**, 702 (1967).
[40]R. M. Clayton, R. S. Rogero, and J. G. Sotter, "An experimental description of destructive liquid rocket resonant combustion," AIAA J. **6**, 1252 (1968).
[41]G. A. Flandro, "Nonlinear unsteady solid propellant flame zone analysis," AIAA Paper 98-3700, Cleveland, OH, 1998. 34th AIAA/ASME/SAE/ASEE Joint Propulsion Conference and Exhibit, 13–15 July.
[42]G. A. Flandro, "Effects of vorticity on rocket combustion stability," J. Propul. Power **11**, 607 (1995).
[43]G. A. Flandro and J. Majdalani, "Aeroacoustic instability in rockets," AIAA J. **41**, 485 (2003).
[44]F. E. C. Culick and V. Yang, "Overview of combustion instabilities in liquid propellant rocket engines," in *Liquid Rocket Engine Combustion Instability*, edited by V. Yang and W. E. Anderson, AIAA Progress in Astronautics and Aeronautics Vol. 169 (AIAA, Reston, VA, 1995), pp. 1–37.
[45]F. E. C. Culick, "A note on Rayleigh's criterion," Combust. Sci. Technol. **56**, 159 (1987).
[46]F. E. C. Culick, "High frequency oscillations in liquid rockets," AIAA J. **1**, 1097 (1963).
[47]G. A. Flandro, "On flow turning," AIAA Paper 95-2530, San Diego, CA, 1995. 31st AIAA/ASME/SAE/ASEE Joint Propulsion Conference and Exhibit, 10–12 July.
[48]G. A. Flandro, W. Cai, and V. Yang, "Turbulent transport in rocket motor unsteady flowfield," in *Solid Propellant Chemistry, Combustion, and Motor Interior Ballistics*, edited by V. Yang, T. B. Brill, and W.-Z. Ren, AIAA Progress in Astronautics and Aeronautics Vol. 185 (AIAA, Washington, DC, 2000), pp. 837–858.
[49]J. Majdalani, G. A. Flandro, and T. S. Roh, "Convergence of two flowfield models predicting a destabilizing agent in rocket combustion," J. Propul. Power **16**, 492 (2000).
[50]J. Majdalani and W. K. Van Moorhem, "Improved time-dependent flowfield solution for solid rocket motors," AIAA J. **36**, 241 (1998).
[51]J. Majdalani, "The boundary layer structure in cylindrical rocket motors," AIAA J. **37**, 505 (1999).
[52]J. Majdalani, "Vorticity dynamics in isobarically closed porous channels. Part I: Standard perturbations," J. Propul. Power **17**, 355 (2001).
[53]J. Majdalani and T. S. Roh, "Vorticity dynamics in isobarically closed porous channels. Part II: Space-reductive perturbations," J. Propul. Power **17**, 363 (2001).
[54]J. Majdalani and T. S. Roh, "The oscillatory channel flow with large wall injection," Proc. R. Soc. London, Ser. A **456**, 1625 (2000).
[55]J. Majdalani, G. A. Flandro, and S. R. Fischbach, "Some rotational corrections to the acoustic energy equation in injection-driven enclosures," Phys. Fluids **17**, 074102 (2005).
[56]F. Vuillot and G. Avalon, "Acoustic boundary layer in large solid propellant rocket motors using Navier-Stokes equations," J. Propul. Power **7**, 231 (1991).
[57]T. S. Roh, I. S. Tseng, and V. Yang, "Effects of acoustic oscillations on flame dynamics of homogeneous propellants in rocket motors," J. Propul. Power **11**, 640 (1995).
[58]T. S. Roh and V. Yang, "Transient combustion response of solid propellant to acoustic disturbance in rocket motors," AIAA Paper 95-0602, Reno, NV, 1995. 33rd Aerospace Sciences Meeting and Exhibit, 9–12 January.
[59]F. Vuillot, "Numerical computation of acoustic boundary layers in large solid propellant space booster," AIAA Paper 91-0206, Reno, NV, 1991. 29th Aerospace Sciences Meeting and Exhibit, 7–10 January.
[60]J. D. Baum, J. N. Levine, and R. L. Lovine, "Pulsed instabilities in rocket motors: A comparison between predictions and experiments," J. Propul. Power **4**, 308 (1988).
[61]J. D. Baum, "Investigation of flow turning phenomenon; effects of frequency and blowing rate," AIAA Paper 89-0297, Reno, NV, 1989. 27th Aerospace Sciences Meeting and Exhibit, 9–12 January.
[62]R. L. Glick and J. P. Renie, "On the nonsteady flowfield in solid rocket

motors," AIAA Paper 84-1475, Cincinnati, OH, 1984. 20th AIAA/SAE/ASME Joint Propulsion Conference, 11–13 June.
[63]R. S. Brown, A. M. Blackner, P. G. Willoughby, and R. Dunlap, "Coupling between acoustic velocity oscillations and solid propellant combustion," J. Propul. Power **2**, 428 (1986).
[64]C. W. Shaeffer and R. S. Brown, "Oscillatory internal flow field studies," United Technologies, AFOSR Contract Report F04620-90-C-0032, San Jose, CA, August 1990.
[65]R. H. Cantrell and R. W. Hart, "Interaction between sound and flow in acoustic cavities: mass, momentum, and energy considerations," J. Acoust. Soc. Am. **36**, 697 (1964).
[66]W. Chester, "Resonant oscillations in closed tubes," J. Fluid Mech. **18**, 44 (1964).
[67]W. A. Sirignano and L. Crocco, "A shock wave model of unstable rocket combustion," AIAA J. **2**, 7 (1964).
[68]G. Kirchoff, *Vorlesungen Über Mathematische Physik: Mechanik*, 2nd ed. (Teubner, Leibzig, 1877).
[69]W. K. Van Moorhem, "Flow turning in solid-propellant rocket combustion stability analyses," AIAA J. **20**, 1420 (1982).
[70]S. Malhotra, "On combustion instability in solid rocket motors," Ph.D. dissertation, California Institute of Technology, 2004.
[71]W. K. Van Moorhem, "An investigation of the origin of the flow turning effect in combustion instability," 17th JANNAF Combustion Conference, Langley, VA, 1980.
[72]J. Majdalani, B. Entezam, and W. K. Van Moorhem, "A novel investigation of the thermoacoustic fields inside a Rijke tube," AIAA Paper 98–2582, Albuquerque, NM, 1998. 7th AIAA/ASME Joint Thermophysics and Heat Transfer Conference, 15–18 June, Albuquerque, New Mexico.
[73]J. Majdalani, B. Entezam, and W. K. Van Moorhem, "The Rijke tube revisited via laboratory and numerical experiments," AIAA Paper 2001-2961, Anaheim, CA, 2001. 35th AIAA Thermophysics Conference, 11–14 June.
[74]B. Entezam, W. K. Van Moorhem, and J. Majdalani, "A full-scale numerical model of the thermoacoustic interactions inside the Rijke tube pulse combustor," Numer. Heat Transfer, Part A **41**, 245 (2002).
[75]F. S. Blomshield and H. B. Mathes, "Pressure oscillations in post-challenger space shuttle redesigned solid rocket motors," J. Propul. Power **9**, 217 (1993).